

Integration of Cholesterol Oxidase-Based Biosensors on a Smart Contact Lens for Wireless Cholesterol Monitoring from Tears

Yang Cui, Lin Zhuo, Yuta Nishina, Saman Azhari, and Takeo Miyake*

Cholesterol plays a critical role in physiological functions, but elevated levels increase the risk of cardiovascular disease. Regular cholesterol monitoring is essential for elderly or obese individuals. Current methods, such as blood tests, are invasive, inconvenient, and require a professional operator. In contrast, tears, as an accessible body fluid, offer a promising alternative for noninvasive monitoring due to their correlation with blood cholesterol levels. Herein, a noninvasive approach for monitoring cholesterol levels in tears using a biosensor integrated into a smart contact lens is reported. The biosensor employs cholesterol oxidases as the biocatalyst, coupled with an osmium-based mediator, to detect cholesterol concentrations ranging from 0.1 mM to 1.2 mM in artificial tears. A key challenge is the extremely low cholesterol concentration in tears, which is addressed using a parity-time (P-T) symmetry-based magnetic resonance coupling system. This system enables wireless signal reading and achieves high sensitivity due to its high-quality (Q) factor, which can achieve a detection limit of 0.061 mM. This portable, high-sensitivity smart contact lens demonstrates significant potential as a wearable device for continuous, noninvasive cholesterol monitoring. The findings contribute to advancing tear-based diagnostic systems and highlight the scientific importance of utilizing tear biomarkers for health monitoring.

Organization statistics in 2019, 32% of the population worldwide died from CVDs.^[2] High blood lipids cause plaque formation on the blood vessel walls, slowing down or even blocking blood flow.^[3] Excessive cholesterol deposits in the blood vessels can lead to atherosclerosis, causing angina pectoris, coronary heart disease, metabolic disorders, and other problems.^[4] Common detection methods can be divided into three types: classical chemical methods based on the Abell–Kendall protocol,^[5] fluorometric and colorimetric enzymatic assays,^[6] and analytical instrumental approaches,^[7] which often require professional institutions such as hospitals or testing centers.^[8] For high-risk groups, regular monitoring of cholesterol levels is necessary.

The rapid development of the electronics industry has led to the emergence of numerous wearable medical devices. Portable and simple medical devices enable individuals to monitor various physiological signals in their bodies continuously. Such devices vary in size, shape, and application, but one of the most commonly used worldwide is

the contact lens, which directly contacts the ocular surface. Developing advanced functions for contact lenses often results in interesting and unexpected outcomes. By eliminating the spatial distance between the device and the eye, simple and effective systems, such as contact lens-based near-eye displays,^[9] continuous fundus phototherapy,^[10] and real-time monitoring of intraocular pressure^[11] have been developed.


Tears, a body fluid that constantly interacts with contact lenses, are secreted outside the body, maintain the normal function and health of the ocular surface, contain a variety of biomarkers, and are easy to sample.^[12] Such features make tears a suitable target for developing noninvasive, portable medical devices, with contact lenses serving as the most promising platform. Currently, some smart contact lenses (SCL) can achieve noninvasive measurement of tear glucose,^[13] cortisol,^[14] matrix metalloproteinase-9 concentration,^[15] etc., to diagnose diseases such as diabetes,^[16] Addison's disease,^[17] dry eyes disease,^[18] meibomian gland dysfunction,^[19] etc. Studies have demonstrated that there is a correlation between cholesterol in tears and the blood,^[20] suggesting the feasibility of noninvasively monitoring cholesterol levels through SCL. Although the tear film consists of lipid, aqueous, and mucin layers,^[21] the free cholesterol content

1. Introduction

Cholesterol plays a critical role in human physiological functions. Higher cholesterol levels of over 5.17 mM will increase the risk of cardiovascular disease (CVD).^[1] According to World Health

Y. Cui, L. Zhuo, S. Azhari, T. Miyake
Graduate school of Information, Production and Systems
Waseda University
2-7 Hibikino, Wakamatsu, Kitakyushu, Fukuoka 808-0135, Japan
E-mail: miyake@waseda.jp

Y. Nishina
Graduate School of Natural Science and Technology
Okayama University
Tsushimaoka, Kita, Okayama 700-8530, Japan

 The ORCID identification number(s) for the author(s) of this article can be found under <https://doi.org/10.1002/aisy.202500368>.

© 2025 The Author(s). Advanced Intelligent Systems published by Wiley-VCH GmbH. This is an open access article under the terms of the Creative Commons Attribution License, which permits use, distribution and reproduction in any medium, provided the original work is properly cited.

DOI: 10.1002/aisy.202500368

is extremely low compared to other lipid components such as cholesterol esters and wax esters,^[22] making the measurement of tear cholesterol extremely challenging.

To simplify the structure of the SCL as much as possible to overcome the size limitations, we selected a chip-less resonant antenna as the sensor and used a wireless system for data read-out. The wireless measurement system is based on a magnetically coupled resonator, including a reader side and a sensor side, as shown in **Figure 1a**. The sensor side is an inductor-capacitor (LC) circuit in parallel with a chemical resistor that can respond to cholesterol concentration, using cholesterol oxidase (ChOxs) together with an Osmium-based mediator (Figure 1b). The cholesterol concentration information in the solution is reflected through the change in resistance Δr , which manifests through amplitude modulation (AM) in the sensor inductor-capacitor-resistor (LCR) resonator (Figure 1c). On the reader side, the traditional lossy LCR resonator exhibits low sensitivity due to its low quality factor (Q-factor), resulting from energy dissipation in the resistor, leading to low sensitivity for detecting small changes in cholesterol concentration. To overcome this, we introduced a P-T symmetry system in the magnetically coupled resonator by using a gain LCR resonator on the reader side. This greatly increases the Q-factor, and consequently the sensitivity, resulting in a linear response to the resistance change Δr on the sensor side.^[23] As a result, this approach enables the detection of low cholesterol concentrations in tears.

2. Results and Discussion

2.1. Cholesterol Oxidase Electrode

Figure 2a shows the multilayer structure of the ChOxs electrode: from inside to outside, carbon fiber (CF), carbon nanotubes (CNTs), PVI-[Os(bpy)₂Cl], and ChOxs. As a mediator molecule, PVI-[Os(bpy)₂Cl] can connect the redox center of the enzyme to the electrode surface, increase the rate of electron transfer to cholesterol oxidase, and improve catalytic efficiency. The

addition of PVI-[Os(bpy)₂Cl] improves the sensor's sensitivity, stability, selectivity, response, and recovery time.^[24] Electrochemical measurement methods were used to evaluate the performance of ChOxs electrodes. The cyclic voltammogram was performed using a three-electrode setup (Figure 2b), where the ChOxs electrode served as the working electrode, the Ag/AgCl (3 M NaCl) acted as the reference electrode, and the platinum wire was used as the counter electrode. The potential was scanned from -0.3 to 0.8 V, and the oxidation reaction was observed to begin at around 0.1 V, reaching a peak near 0.3 V. The height of this oxidation peak increased with the increase in cholesterol concentration. To confirm the correlation between the response current of the ChOx electrode and the cholesterol concentration, chronoamperometry was performed. A potential of 0.8 V was applied between the working electrode and the counter electrode,^[25] and the oxidation current was measured (Figure 2c). The current change in response to cholesterol concentration, ranging from 0.0 to 1.0 mM with a 0.2 mM step, and from 1.0 to 3.0 mM with a 1.0 mM step. The response showed linear correlation to varying cholesterol concentration with a sensitivity of $2.41 \mu\text{A mM}^{-1}$. In addition, the selectivity of the fabricated sensor toward other molecules present in tears, such as lactic acid, urea, and glucose, was investigated.^[26] As shown in Figure 2d, the baseline current remained unchanged upon the addition of these molecules (lactic acid, urea, and glucose), whereas the addition of cholesterol led to an increase in current. These results indicated the substrate specificity of using our enzyme-based sensors with high sensitivity for cholesterol detection.

To verify the biosafety of the ChOxs electrode, human corneal cells were cultured in the same dish as the prepared CF electrode, and the viability of the cells after 24 h, 48 h, and 72 h was observed. A statistical T-test was conducted on the obtained results using Excel software. As shown in Figure S1a, Supporting Information, there was no significant difference between the control and experimental groups ($p > 0.05$), and the viability remained more than 99% after three days. Figure S1b, Supporting Information, shows the image of the original cells, the cells stained with Calcein-AM for living cells and propidium iodide for dead cells. We mainly focus on the area

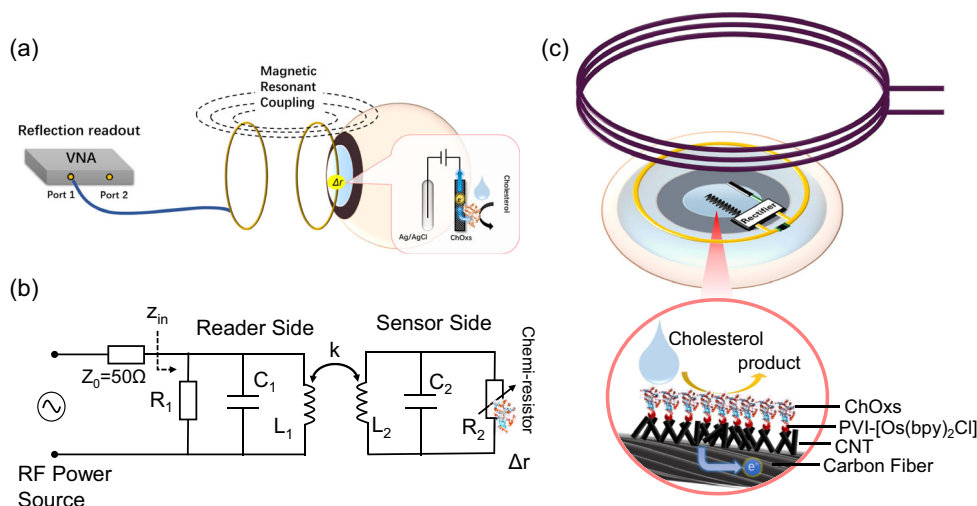


Figure 1. Wireless cholesterol measurement system. a) The measurement setup. b) The schematic of the magnetic coupling resonator. c) The working principle of the cholesterol wireless measurement system.

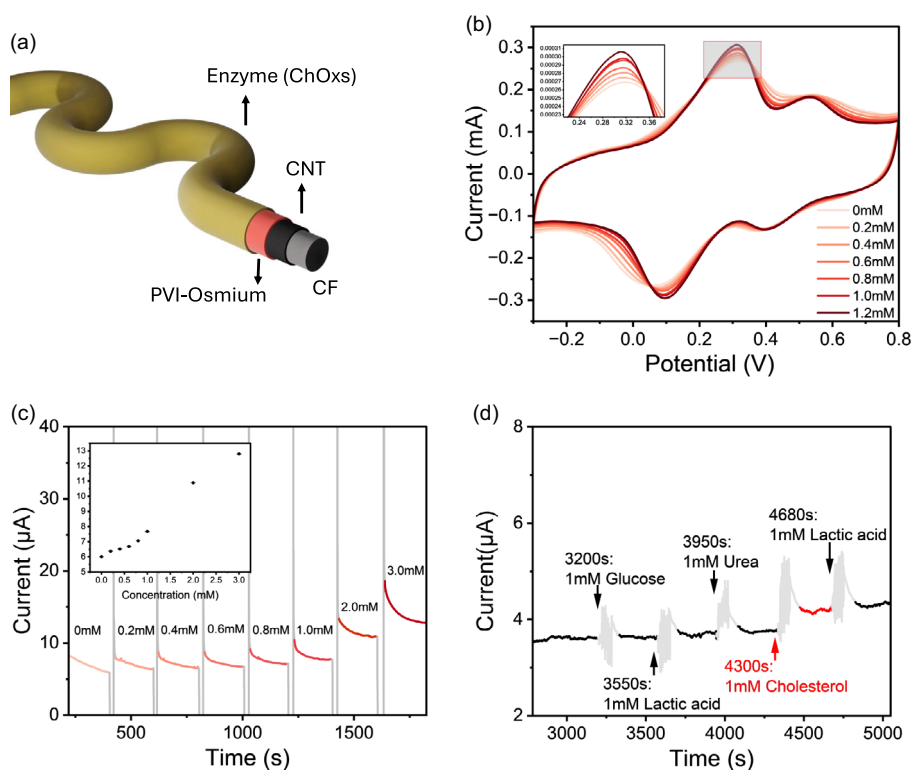


Figure 2. a) The multilayer structure of the ChOx electrode. b) The cyclic voltammogram of the ChOx electrode at fixed cholesterol concentration (0 mM \approx 1.2 mM). Scan potential: $-0.3 \approx 0.8$ V. The inset is an enlarged image of the gray box. c) The chronoamperometry of different cholesterol concentrations measured by the ChOx electrode versus Ag/AgCl (NaCl, 3 M) at 0.8 V. The gray area is the transition time for changing the cholesterol solution. The relationship between the cholesterol concentration and oxidation current is shown in the inset. The error bars represent the standard deviation of three different samples ($n = 3$). d) The chronoamperometry of different interferents of equal concentration. The gray area is the transition time for stirring the solution until it becomes uniform.

where the ChOx electrode is in contact with the cell, which is the black area in Figure S1b, Supporting Information. From these images, it is evident that the presence or absence of the electrode does not affect the growth and viability of the corneal cells.

2.2. Biosensor

Figure 3a shows the schematic of the biosensor. The variable resistor is a chemical resistor with a dual-electrode structure, with one side being a CF with the ChOx fixed as the working electrode and the other an Ag/AgCl electrode as the counter electrode. The full-bridge rectifier is used to convert the wirelessly transmitted AC into DC in parallel with the smoothing capacitor (C_{smooth}). At this stage, the oxidation current is supplied to the enzyme electrode. The variation in cholesterol concentration on the electrode causes the oxidation current to change. Therefore, the entire circuit as a whole can be regarded as a variable resistor based on cholesterol concentration. **Figure 3b** shows a physical sensor structure with the LCR resonant circuit. The ChOx-based chemical resistor is connected in parallel with the inductive copper antenna (L) and the capacitor (C). This setup is directly connected to the vector network analyzer (VNA) to measure the change of the real part of the impedance $Re(Z_L)$ at the resonance frequency. **Figure 3c** shows the peak at the resonance frequency

of 90.7 MHz for the LC resonator in parallel with the cholesterol biosensor. When the cholesterol concentration increases from 0 to 1.2 mM, the value of $Re(Z_L)$ gradually decreases from 1168.89 ± 0.27 to $1154.94 \pm 2.22 \Omega$, respectively. This is because the increase in cholesterol concentration increases the anode reaction rate, hence increasing the current at the interface between the bioanode and the solution and reducing the resistivity between the ChOx bioanode and the Ag/AgCl cathode. This means that the cholesterol biosensor can respond to cholesterol concentration and achieve AM at the resonant frequency with a sensitivity of $11.6 \Omega \text{ mM}^{-1}$.

2.3. Wireless Cholesterol Measurement

Our wireless measurement system includes a sensor side and a reader side (**Figure 4a**). The reader side is an LCR resonator with parallel configuration, connected to a VNA to measure the input impedance $Re(Z_{\text{in}})$. The traditional reader is a loss LCR resonator, in which the energy dissipation occurs at the resistor, resulting in a reduced Q-factor and weak biological signal detection. In contrast, our previous work proposed a gain LCR resonator based on the P-T symmetric principle.^[23] By setting the reader side resistance to $-R$ (**Figure 4a**), —that is, creating a negative resistance whose magnitude equals the positive loss resistance R on

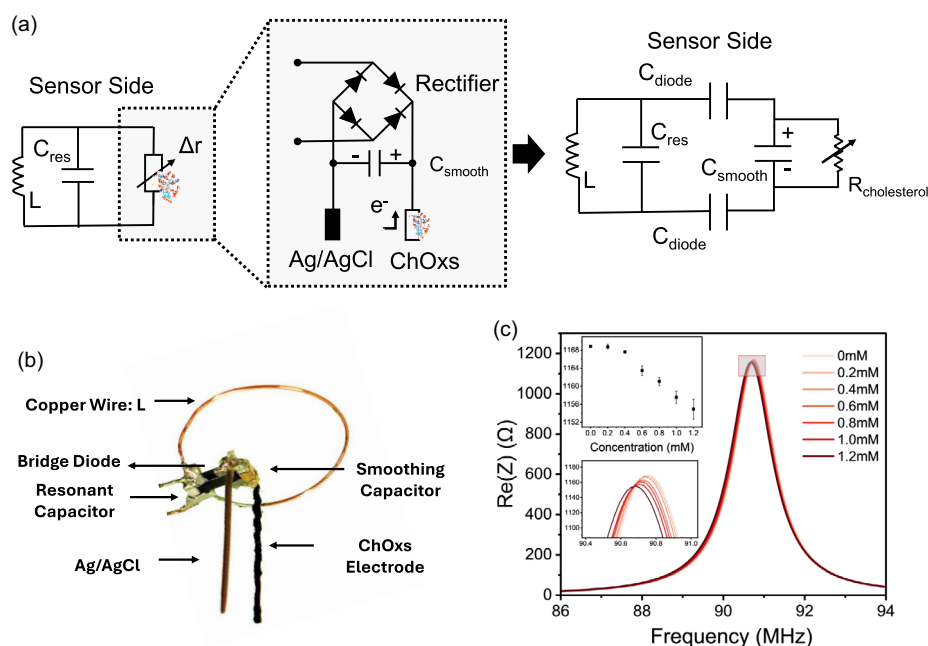


Figure 3. a) The working principle of the variable resistor of the biosensor. Left: circuit schematic of the sensor side, right: equivalent circuit schematic of the entire sensor side. b) The physical image of the sensor side with the LCR resonant circuit. Vertically connecting the ChOxs electrode and Ag/AgCl simplifies the initial evaluation of the device in various concentrations of cholesterol solutions. c) Real part of the input impedance $Re(Z_L)$ versus frequency of biosensor at different cholesterol concentrations (0 \approx 1.2 mM). The plot of $Re(Z_L)$ versus cholesterol concentration is depicted in the upper inset. The lower inset is the enlarged image of the gray box. The error bars represent the standard deviation of three different samples ($n = 3$).

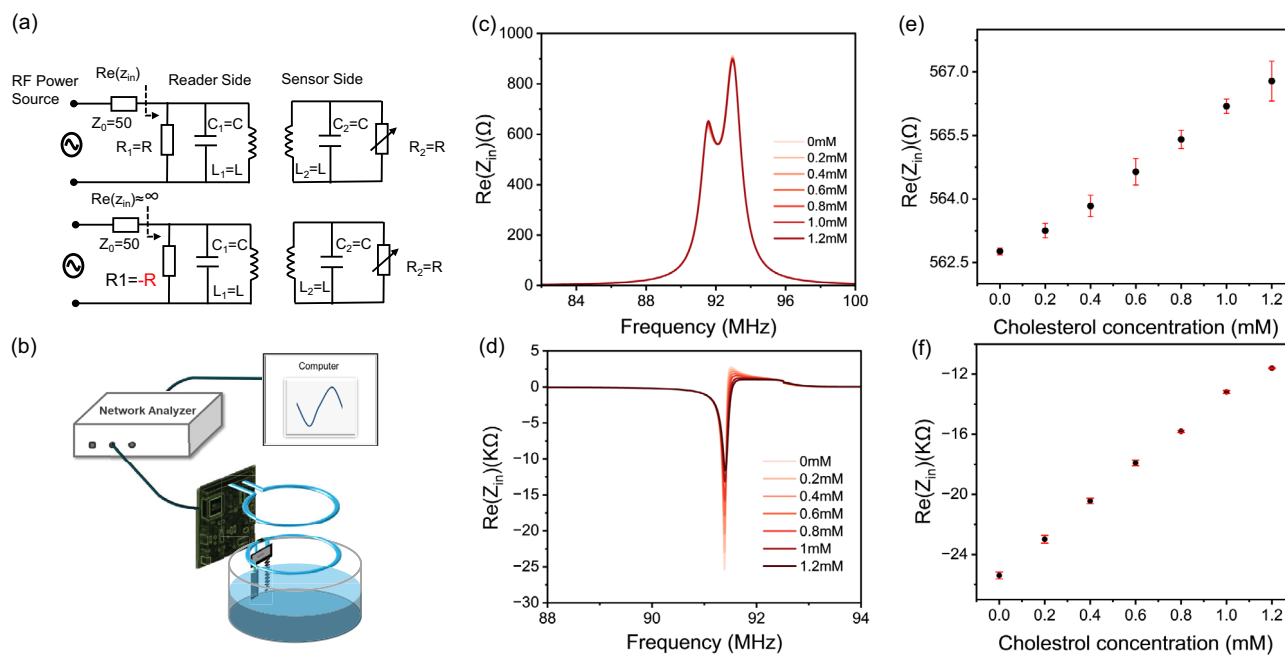


Figure 4. a) Simplified magnetic resonant coupling system circuit diagram. Top: traditional loss-loss system, bottom: P-T symmetric (gainloss) system. b) The measurement setup for wireless monitoring of cholesterol level. The real part of the input impedance, $Re(Z_{in})$ versus frequency of the reader resonator coupled with the cholesterol biosensor at fixed cholesterol concentrations (0 \approx 1.2 mM) measured by c) the conventional and d) broken P-T symmetric system. e,f) The plots of $Re(Z_{in})$ versus cholesterol concentration. The error bars represent the standard deviation of three different samples ($n = 3$).

the sensor side—we balance gain and loss, reduce the energy dissipation, increase the Q-factor, and thereby improve the sensitivity. The exceptional point (EP) in the P-T symmetric

system is a specific point where eigenvalues and eigenvectors of the non-Hermitian Hamiltonian system coalesce. When the coupling coefficient k of the P-T symmetric system is set to

be smaller than the k value at the EP, the broken P-T symmetric system occurs. At this time, the reader side will show a linear response to the disturbance (Δr) on the sensor side. The specific details can be found in previous work.^[23] Figure 4b shows the setup of the measurement. Using this system, not only does the sensitivity greatly improve, but also the linearity of the response improves, and hence, the analysis of the measurement results becomes simpler and more accurate.

Figure 4c,d shows the wireless measurement results of various concentrations of cholesterol solutions by using the conventional (loss-loss) system and the broken P-T symmetric (gain-loss) system, respectively. In these experiments, we fabricated three identical enzyme electrodes, which were used for measurement while ensuring that the test samples and experimental settings remained unchanged to ensure the stability and reproducibility of the experiment. The reader of the conventional system is fixed at 14.9 mm from the sensor. There are two peaks present at 91.57 MHz and 92.94 MHz, which are due to the mode splitting caused by strong resonant coupling. At the resonant frequency of about 92 MHz, as the cholesterol concentration increases from 0 to 1.2 mM, the average value of $Re(Z_{in})$ gradually increases from 562.77 ± 0.08 to $566.78 \pm 0.47 \Omega$, respectively, with a sensitivity of about $3.3 \Omega/\text{mM}$ and a limitation of detection (LOD) of 0.15 mM. Although the impedance values $Re(Z_{in})$ show a linear relationship with the change in concentration, the extremely low sensitivity suggests that the practical operation is unfeasible. In contrast with the broken P-T symmetry system, as the cholesterol concentration increases from 0 to 1.2 mM, at the resonant frequency of 91.40 MHz, the average values of $Re(Z_{in})$ change from $-25.40 \times 10^3 \pm 0.23 \times 10^3$ to $-11.61 \times 10^3 \pm 0.031 \times 10^3 \Omega$, respectively. The broken P-T symmetry reader coil is fixed at 15 mm from the sensor. As shown in Figure 4d, the broken P-T symmetric system exhibits a linear response to the disturbance (Δr) of the chemical resistor with a LOD of 0.061 mM and a sensitivity of $11.5 \times 10^3 \Omega/\text{mM}$, which is 3480 times higher and significantly greater than the result of the loss-loss configuration observed in the traditional system.

2.4. Wireless Measurements of Yolk Samples

To investigate the feasibility of the sensor as an SCL, a contact lens equipped with a ChOx biosensor was fabricated, and the P-T symmetric system was used to monitor cholesterol concentration wirelessly. Figure 5a shows a physical picture of the SCL. A commercial portable blood lipid meter (MLA-1, Zealson Bio-Technology, China) was used as a benchmark to compare with the results obtained from SCL. Since the commercial blood lipid meter only measures the blood cholesterol concentration range, the cholesterol concentration below 2.59 mM and over 10.35 mM is immeasurable. The biological sample is the yolk from five kinds of eggs purchased from the market. Every 100 g of egg yolk contains 1510 mg of cholesterol.^[27] We took 1.0 g of egg yolk and added 5 mL Phosphate Buffered Saline (PBS, 0.1 M, PH 7.0) solution to obtain the yolk sample with a theoretical cholesterol concentration of 6.5 mM. The cholesterol concentration was measured using a commercial blood lipid meter and our SCL. As shown in Figure 5b, the results measured by the commercial blood lipid meter are 4.28, 4.85, 5.11, 5.01, and 5.15 mM for five different eggs. The results measured by

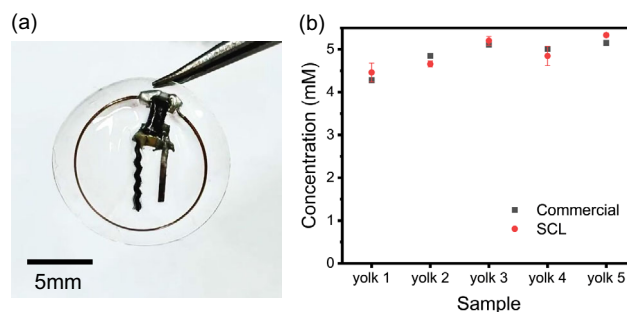


Figure 5. a) The fabricated SCL device for biological sample testing. b) The cholesterol concentration measurement of five different egg yolks by the SCL and a commercial blood lipid meter. The error bars represent the standard deviation of three different samples ($n = 3$).

SCL are 4.46 ± 0.22 mM, 4.65 ± 0.07 mM, 5.20 ± 0.10 mM, 4.85 ± 0.23 mM, and 5.33 ± 0.05 mM for the same samples tested with the commercial blood lipid meter. It is evident that even at higher cholesterol concentrations, our measurement results are still consistent with those of the commercial device. Both devices can reflect the difference in the cholesterol content of the five egg yolks.

3. Conclusion

We have developed an SCL that can wirelessly measure cholesterol concentration in artificial tears and egg yolk. This highly selective SCL can measure extremely low cholesterol concentrations (0.1 mM - 1.2 mM). By taking advantage of the P-T symmetry principle, we have increased the sensitivity of the wireless measurement system by 3480 times with stable linearity within the measurement range, improving the accuracy of the measurement. Even in biological samples, the measurement results of our SCL are consistent with those of a commercial blood lipid meter. Portable and accurate wireless measurement of tear cholesterol means that ordinary people can easily monitor their health condition with continuity. As a wearable device that can transmit signals wirelessly, our SCL will have the opportunity to connect with intelligent systems. The integration and continuous collection of various biological information, including cholesterol, will make the judgment on human health status more specific and personalized, that is, more intelligent, which also means that our system has great potential in the field of intelligent medical devices.

4. Experimental Section

Fabrication of ChOx Electrode: The fabrication process of ChOx electrode utilized was as follows: drop 20 μL 0.1% CNT solution (TUBALL SWCNT) was added onto a 5 mm CF and dried on a hotplate at 80 °C for 10 min; the process was repeated three times, and then the CNT-coated CF was washed in distilled water for 30 min. Next, the CNT-coated CF was soaked in a 1.5 mg mL^{-1} PVI-[Os(bpy)₂Cl] buffer solution (PBS, 0.1 M, PH 7.0) at 4 °C for 2 h, and then PVI-[Os(bpy)₂Cl]-coated electrode was washed with a buffer solution (PBS, 0.1 M, PH 7.0) for 30 min. The PVI-[Os(bpy)₂Cl] was provided by the Nishina Yuta laboratory at Okayama University. Finally, we soaked the treated CF in a 4 mg/mL ChOx buffer

solution (PBS, 0.1 M, PH 7.0) at 4 °C for 2 h to obtain an enzyme electrode with a multilayer structure: CF/CNT/ PVI-[Os(bpy)₂Cl]/ChOxs.

Fabrication of Gain LCR Resonator in Broken P-T Symmetric System: The fabrication of the gain LCR resonator for the reader side of the broken P-T symmetric system was done by printed circuit board (PCB) fabrication technology (Figure S2a, Supporting Information). First, the resonant LCR circuit was designed to determine the locations of the components. Second, the circuit diagram was transferred to the PCB substrate by photolithography. The excess resist coating was then dissolved using NaOH to expose the non-circuit copper layer. Finally, the noncircuit area of the copper layer was etched by the FeCl₂ solution through a replacement reaction, leaving the designed circuit pattern. After that, the fabrication of the gain LCR resonator was completed by drilling holes in the PCB board and soldering the electronic components. The circuit uses a Clapp oscillator to achieve negative resistance, as shown in Figure S2b, Supporting Information. The parameters of the electronic components were: Bipolar junction transistor (c1815), inductor ($L_1 = 32\text{ nH}$), source resistor ($R_3 = 120\ \Omega$), bias resistor ($R_1 = 4.7\ \text{k}\Omega$, $R_2 = 2.2\ \text{k}\Omega$), source capacitor ($C_1 = 120\ \text{pF}$), bypass capacitor ($C_2 = 220\ \text{pF}$, $C_3 = 100\ \text{pF}$), and oscillation capacitor ($C_4 = 50 + 10 \approx 50\ \text{pF}$, $C_5 = 150\ \text{pF}$, $C_6 = 150\ \text{pF}$). The SMA connector was connected at both ends of L_1 . By adjusting the oscillation capacitor, the final resonant frequency of our circuit was set to $\approx 91\ \text{MHz}$.

Fabrication of Biosensor Resonator: The biosensor resonator (Figure 3a) included a copper coil ($L = 32\ \text{nH}$, coil diameter: 12 mm, wire diameter: 0.238 mm), a resonant capacitor ($C_{\text{res}} = 100\ \text{pF}$), a bridge rectifier diode (BAS4002A-RPP, $C_{\text{diode}} = 2 \approx 5\ \text{pF}$), a smoothing capacitor ($C_{\text{smooth}} = 22\ \mu\text{F}$), a CF electrode with immobilized ChOxs, and an Ag/AgCl electrode. When the reader was coupled to the sensor, the AC voltage was received and then converted into a DC voltage through the rectifier circuit. Therefore, a stable DC voltage between the ChOxs and the Ag/AgCl electrode were obtained. The electron transfer on the ChOxs electrode is related to the cholesterol concentration and can, therefore, be expressed as a chemical resistance $R_{\text{cholesterol}}$.

Fabrication of Smart Contact Lens: The contact lens was made of polydimethylsiloxane (PDMS). A mixed solution of a Sylgard 184 silicone elastomer kit was poured into a hemisphere mold, and then the receiver coil, along with the cholesterol biosensor, was placed at the center of the mold. After pouring the elastomer liquid onto the device-mounted mold, it was placed in a 35 °C environment until it solidified. Finally, the PDMS on the surface of the enzyme electrode and Ag/AgCl electrode area was removed with a scraper to enable them to be exposed to artificial tear fluid.

Supporting Information

Supporting Information is available from the Wiley Online Library or from the author.

Acknowledgements

This work was supported by AMED under grant no. JP23hma322020, the Canon Foundation and Japan Society for the Promotion of Science (Grant-in-Aid for Scientific Research A): 24H00805. Part of this work was conducted at Kitakyushu Foundation for the Advancement of Industry, Science and Technology, Semiconductor Center, supported by "Nanotechnology Platform Program" of the Ministry of Education, Culture, Sports, Science and Technology (MEXT), Japan.

Conflict of Interest

The authors declare no conflict of interest.

Data Availability Statement

The data that support the findings of this study are available from the corresponding author upon reasonable request.

Keywords

cholesterol, magnetic resonance coupling, parity-time symmetry, smart contact lens

Received: March 31, 2025

Revised: May 17, 2025

Published online:

- [1] a) S. M. Grundy, J. I. Cleeman, C. N. B. Merz, H. B. Brewer, L. T. Clark, D. B. Hunninghake, R. C. Pasternak, S. C. Smith, N. J. Stone, *Circulation* **2004**, *110*, 227; b) D. S. Schade, L. Shey, R. P. Eaton, *Endocr. Pract.* **2020**, *26*, 1514; c) J. M. Ordovas, *Am. J. Clin. Nutr.* **2009**, *89*, 1509S; d) J. D. James, H. O. K. James, *Open Heart* **2018**, *5*, e000871; e) J. F. Trejo-Gutierrez, G. Fletcher, *J. Clin. Lipidol.* **2007**, *1*, 175; f) I. Tabas, *J. Clin. Invest.* **2002**, *110*, 583.
- [2] World Health Organization, Cardiovascular diseases (CVDs), [https://www.who.int/news-room/fact-sheets/detail/cardiovascular-diseases-\(cvds\)](https://www.who.int/news-room/fact-sheets/detail/cardiovascular-diseases-(cvds)) (accessed: June 2021).
- [3] H. Ma, K.-J. Shieh, *J. Am. Sci.* **2006**, *2*, 46.
- [4] M. Grundy Scott, *J. Am. Coll. Cardiol.* **2006**, *47*, 1093.
- [5] L. Abell, B. Levy, B. Brodie, F. Kendall, *J. Biol. Chem.* **1952**, *195*, 357.
- [6] D. M. Amundson, M. Zhou, *J. Biochem. Biophys. Methods* **1999**, *38*, 43.
- [7] M. Heuillet, B. Lalere, M. Peignaux, J. De Graeve, S. Vaslin-Reimann, J.-P. Pais De Barros, P. Gamber, L. Duviard, V. Delatour, *Clin. Biochem.* **2013**, *46*, 359.
- [8] L.-H. Li, E. P. Dutkiewicz, Y.-C. Huang, H.-B. Zhou, C.-C. Hsu, *J. Food Drug Anal.* **2019**, *27*, 375.
- [9] a) Y. Wu, C. P. Chen, L. Mi, W. Zhang, J. Zhao, Y. Lu, W. Guo, B. Yu, Y. Li, N. Maitlo, *Opt. Express* **2018**, *26*, 11553; b) J. Chen, L. Mi, C. P. Chen, H. Liu, J. Jiang, W. Zhang, *Opt. Express* **2019**, *27*, 38204.
- [10] a) G.-H. Lee, C. Jeon, J. W. Mok, S. Shin, S.-K. Kim, H. H. Han, S.-J. Kim, S. H. Hong, H. Kim, C.-K. Joo, J.-Y. Sim, S. K. Hahn, *Adv. Sci.* **2022**, *9*, 2103254; b) C. A. Cook, J. C. Martinez-Camarillo, Q. Yang, N. E. Scianmarello, M. S. Humayun, Y. C. Tai, 2018 IEEE Micro Electro Mechanical Systems (MEMS), 21-25 Jan. 2018, **2018**.
- [11] a) S. C. Xu, A. C. Gauthier, J. Liu, *J. Ophthalmol.* **2016**, *2016*, 4727423; b) G.-Z. Chen, I.-S. Chan, L. K. K. Leung, D. C. C. Lam, *Med. Eng. Phys.* **2014**, *36*, 1134.
- [12] M. D. Willcox, *Clinical and Experimental Optometry* **2019**, *102*, 350.
- [13] J. Park, J. Kim, S.-Y. Kim, W. H. Cheong, J. Jang, Y.-G. Park, K. Na, Y.-T. Kim, J. H. Heo, C. Y. Lee, J. H. Lee, F. Bien, J.-U. Park, *Sci. Adv.* **2018**, *4*, eaap9841.
- [14] M. Ku, J. Kim, J.-E. Won, W. Kang, Y.-G. Park, J. Park, J.-H. Lee, J. Cheon, H. H. Lee, J.-U. Park, *Sci. Adv.* **2020**, *6*, eabb2891.
- [15] J. Jang, J. Kim, H. Shin, Y.-G. Park, B. J. Joo, H. Seo, J.-e. Won, D. W. Kim, C. Y. Lee, H. K. Kim, J.-U. Park, *Sci. Adv.* **2021**, *7*, eabf7194.
- [16] R. Klein, B. E. K. Klein, S. E. Moss, K. J. Cruickshanks, *Arch. Ophthalmol.* **1994**, *112*, 1217.
- [17] O. Edwards, J. M. Galley, R. J. Courtenay-Evans, J. Hunter, A. Tait, *The Lancet* **1974**, *304*, 549.
- [18] J. L. Gayton, *Clin. Ophthalmol.* **2009**, *3*, 405.
- [19] S. Sabeti, A. Kheirikhah, J. Yin, R. Dana, *Surv. Ophthalmol.* **2020**, *65*, 205.
- [20] H. Song, H. Shin, H. Seo, W. Park, B. J. Joo, J. Kim, J. Kim, H. K. Kim, J. Kim, J.-U. Park, *Adv. Sci.* **2022**, *9*, 2203597.
- [21] S. Masoudi, *Exp. Eye Res.* **2022**, *220*, 109101.
- [22] a) A. H. Rantamäki, T. Seppänen-Laakso, M. Oresic, M. Jauhiainen, J. M. Holopainen, *PLOS ONE* **2011**, *6*, e19553; b) X. E. Wei, J. Korth, S. H. J. Brown, T. W. Mitchell, R. J. W. Truscott, S. J. Blanksby,

- M. D. P. Willcox, Z. Zhao, *Invest. Ophthalmol. Visual Sci.* **2013**, 54, 8027.
- [23] T. Takamatsu, Y. Sijie, T. Miyake, *Adv. Mater. Technol.* **2023**, 8, 2201704.
- [24] S. Yoshino, T. Miyake, T. Yamada, K. Hata, M. Nishizawa, *Adv. Energy Mater.* **2013**, 3, 60.
- [25] L. E. Doyle, E. Marsili, *Bioresour. Technol.* **2015**, 195, 273.
- [26] a) D. Pankratov, E. González-Arribas, Z. Blum, S. Shleev, *Electroanalysis* **2016**, 28, 1250; b) A. Y. Chang, B. Purt, *Biochemistry, Tear Film*, StatPearls Publishing, Treasure Island (FL), **2023**.
- [27] J. Chen, B. Pei, S. Shi, *Poult. Sci.* **2025**, 104, 104660.